COMBUSTION SIMULATIONS OF SCRAMJET COMBUSTOR USING REDUCED MECHANISM OF SURROGATE FUEL FOR REGENERATIVE COOLING PYROLYSIS PRODUCTS

by

Zhongwen LI[a,b], Jingbo WANG[a,b*], and Xiangyuan LI[a,b]

[a] School of Chemical Engineering, Sichuan University, Chengdu, China
[b] Engineering Research Center of Combustion and Cooling for Aerospace Power, Ministry of Education, Sichuan University, Chengdu, China

Original scientific paper
https://doi.org/10.2298/TSCI231223114L

Taking the surrogate fuel (64% ethylene and 36% methane in mole percentage) for regenerative cooling pyrolysis products used in HIFiRE-2 scramjet combustor as an example, present work systematically explores the workflow of the integrated mechanism reduction for surrogate fuel of pyrolysis products, the kinetic performance verification of the preferred reduced mechanism, and the combustion simulation application of the reduced mechanism in scramjet combustor. A static integrated reduction strategy is performed to obtain reduced mechanism for the surrogate fuel with the NUIGMech1.2 as detailed mechanism under wide conditions for temperature range of 900-1800 K, pressure range of 1-4 atmosphere, and equivalence ratio range of 0.25-5.0. A reduced mechanism (34 species and 181 reactions) with remarkably reduced size is obtained, which presents favorable performance in comprehensive kinetic validations. With this compact and high-fidelity reduced mechanism, the combustion simulations for the scramjet combustor are carried out combining with tabulation of dynamic adaptive chemistry for run-time speed-up. The simulation results of static pressure profiles obtained for cold and hot states match well with the experimental measurements for the two conditions with flight Mach number of 5.84 and 6.50. Meanwhile, the flow and combustion characteristics of the two conditions are investigated based on simulation results. The integrated reduction strategy and systematic kinetic verification used in present work provide reference values for the application of more complex surrogate fuel mechanisms in scramjet combustor combustion simulation.

Key words: *pyrolysis products, surrogate fuel, integrated reduction strategy, reduced mechanism, scramjet combustor, combustion simulation*

Introduction

As the increase in flight speed and time, the thermal environment of scramjet engines becomes even harsher, thermal protection issue increasingly become a technological bottleneck for reliable operation of scramjet engines [1]. Regenerative cooling is one of the key technologies of thermal protection for scramjet combustor, which uses onboard liquid endothermic hydrocarbon fuel as cooling medium [2, 3]. Fuel such as aviation kerosene first flows through cooling channels surrounding the combustor and carries heat away from wall *via* convection

* Corresponding author, e-mail: wangjingbo@scu.edu.cn

heat transfer and endothermic reactions [4]. As pyrolysis occurs, large molecules of fuel decompose into small molecule hydrocarbons and hydrogen [2, 3, 5]. Previous studies on pyrolysis of aviation fuels have shown high total molar fraction of ethylene and methane [2, 3, 5], they bound the range of ignition delay times associated with hydrocarbon fuels over a broad range of operating conditions [6]. Thus, hypersonic international flight research experimentation flight 2 (HIFiRE-2) [7, 8] adopted an surrogate fuel with a binary blend of 64% ethylene and 36% methane (in mole percentage) to characterize the ignition and flameholding characteristics of partially-cracked JP-7 [9]. Given that the HIFiRE-2 scramjet combustor adopts a relatively simple pyrolysis product surrogate fuel, and has relatively detailed configuration parameters and experimental data from ground direct-connect rig platform, it is well suited for the study of mechanism reduction methods for surrogate fuel, kinetic performance verification scheme for preferred reduced mechanism, and the application of reduced mechanism in combustion simulation of scramjet combustor.

A variety of detailed kinetic models related to the combustion of small molecules (C_0-C_4) of hydrogen and hydrocarbon fuels are developed in recent decades [10-14]. Among them, the NUIGMech1.2 [14] including 2,857 species and 11,814 reactions can well characterize the combustion and pyrolysis characteristics for single-component and multi-component blended fuels under wide working conditions [14-17]. However, its large size leads to prohibitive computational cost and brings stiff problem to numerical solution [18]. To facilitate the application of fuel mechanism in combustion simulation of combustors, many static mechanism reduction methods are developed in recent years to obtain reduced mechanism without sacrificing accuracy on relevant combustion characteristics within a certain range of operating conditions [18, 19]. Direct relation graph (DRG) related methods yield a good compromise between reduction accuracy and computational cost, hence they are often employed first in multi-stage reductions [18, 19]. Xue *et al.* [19] recently proposed the path flux analysis with error propagation (PFAEP) method, this method presents excellent performance among six DRG-related methods in the reduction of isobutene [18, 19]. Sensitivity analysis (SA) based methods usually eliminate unnecessary species in uncertain species set derived by DRG-related methods, and these methods are created to efficiently aid reduction process [18, 20]. The traditional SA methods need to iteratively compute the sensitivity coefficients of species to eliminate unnecessary species, resulting in very high computational cost [20]. Xi *et al.* [20] improved SA based method by firstly identifying of strongly-coupled species pairs and then performing incremental species deletion. As demonstrated in the reduction of *n*-heptane mechanism, the computational cost is greatly decreased [20]. After the stages of species elimination reduction, mechanisms can be further reduced by eliminating unimportant reactions. Lu and Law [21] developed the reaction elimination method based on the computational singular perturbation (CSP) importance index. Considering each reduction method is tailored for a specific reduction stage, integrated strategies are preferred in mechanism reduction process, which are proved to be reliable and efficient to achieve maximal reduction of many fuels [21-23]. Additionally, the tabulation of dynamic adaptive chemistry (TDAC) method is proved to be promising in decreasing prohibitive computational cost in combustion simulation of combustors with reduced or detailed mechanisms [24-27]. The dynamic adaptive chemistry (DAC) method acquires local reduced mechanism at ru*n*-time, and the in-situ adaptive tabulation (ISAT) algorithm tabulates and reuses previously solutions [24-26]. Li *et al.* [25] evaluated the speed-up performance of different dynamic reduction methods with ISAT turned on for reduced and detailed mechanisms of natural gas and biogas in combustion simulation of Delft jet in hot co-flow burner, and found that elementary flux analysis (EFA) [28] presents superior performances.

Some researchers have carried out mechanism reduction for small molecule fuels, However, the reduced mechanism applicable for multi-component fuels is larger in size, and fewer mechanisms are specialized for dual fuel of methane and ethylene. Sharma *et al.* [29] yielded a skeletal mechanism for high temperature combustion of H_2/CO/C_1-C_4 compounds with 50 species and 373 reactions by reducing USC Mech-II [11]. Xue *et al.* [19] derived a skeletal mechanism suitable for oxidation of hydrocarbon and oxygenated C_0-C_4 fuels under wide range of conditions containing 149 species and 925 reactions by performing reductions for AramcoMech 3.0 [30]. Luo *et al.* [31] achieved a skeletal mechanism for ethylene/methane mixtures with excessive NO enrichment consisting of 44 species and 269 reactions by reducing an integrated mechanism of USC Mech-II [11] and GRI-Mech 3.0 [13]. Concerning the combustion simulation of HIFiRE-2 combustor, based on the detailed mechanism GRI-Mech 3.0 (53 species and 325 reactions) [13], Saghafian *et al.* [32] conducted a large eddy simulation study using compressible flamelet/progress variable approach. In the Reynolds-averaged Navier-Stokes simulations [7, 33], a reduced Taitech-Princeton ethylene model of 22 species and over 200 reactions was developed based on the mechanism of Wang and Laskin [10]. However, more details about this specialized mechanism are not provided. Therefore, it is necessary to propose a compact and comprehensively validated reduction mechanism specialized for dual fuel of methane and ethylene.

Given the promising application of regenerative cooling technology for scramjet combustor and the lack of integrated reduction strategy for surrogate fuel of pyrolysis products, present work aims to explore the whole workflow from the integrated reduction of surrogate fuel, comprehensive kinetic performance verification of preferred reduced mechanism, to the combustion simulation application of the mechanism in scramjet combustor. Based on the development of mechanism reduction methods in recent years, a static integrated reduction strategy is proposed and performed to obtain a high-fidelity reduced mechanism of surrogate fuel with NUIGMech1.2 [14] as the detailed mechanism. To ensure the reliability of obtained reduced mechanism, systematic validations are conducted on kinetic characteristics. Combined with the TDAC method [24], this mechanism is applied to the combustion simulations of HIFiRE-2 scramjet combustor. Then the flow and combustion characteristics are investigated according to the results of combustion simulations under two conditions with flight Mach number of 5.84 and 6.50.

Computational specifications

Static reduction set-up

The flowchart of the static integrated reduction strategy with NUIGMech1.2 [14] as the detailed mechanism is illustrated in fig. 1. Mechanism extraction and clean-up is first carried out to extract sub-mechanism of species with carbon number ≤ 4 (including H_2 mechanism) and clean unnecessary sub-mechanisms of NO_x and NH_3. According to the operating conditions of HIFiRE-2 scramjet combustor [7, 8], the temperature range of 900-1800 K, pressure range of 1-4 atmosphere, and equivalence ratio range of 0.25-5.0 are chosen as the target reduction conditions. Two stages species elimination are performed in sequence by the cost-effective PFAEP [19] method and the relatively costly but efficient improved SA method [20], followed by further reaction elimination based on the CSP importance index [21]. Systematic kinetic verifications are then conducted on the preferred reduced mechanism intended for combustion simulation to check its reliability. These kinetic verifications, including ignition delay times

(IDT), laminar flame speeds (LFS), species concentration profiles (SCP), adiabatic flame temperature profiles (AFTP) and "S"-curves, are performed by the Chemkin-pro package [34]. Present integrated skeletal reduction is performed by the automatic mechanism reduction program ReaxRed [19, 35] adopting the relative error of IDT as the indicator, which has proven to be effective in extensive reduction practices [19-21].

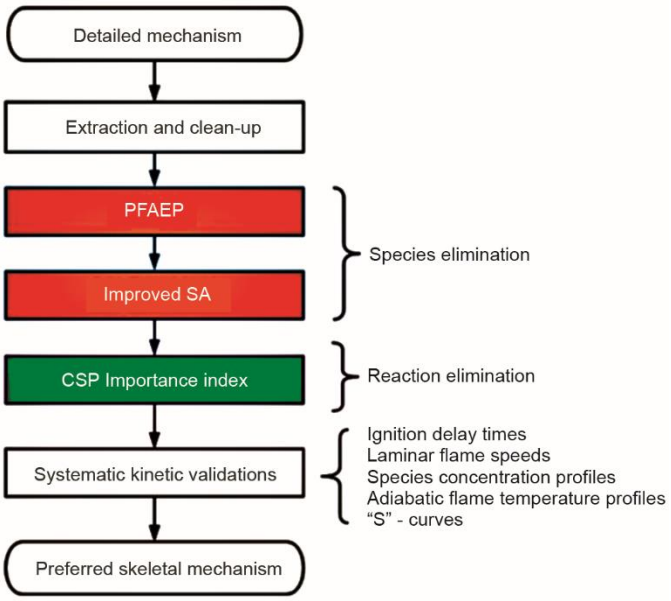

Figure 1. The integrated reduction strategy adopted for mechanism reduction and verification scheme for preferred reduced mechanism

Computational domain and boundary conditions

The structure and experimental measurement data of investigated model scramjet combustor are taken from the relevant researches of HIFiRE-2 [7, 8, 36]. As shown in fig. 2(a), the whole scramjet combustor consists of an isolator (equal-area of 101.6 mm × 25.4 mm) section of 203.2 mm in length, and a combustor section dominated by two symmetrically distributed cavities of 508.1 mm in length with unilateral expansion angle of 1.3°. The fuel is injected into the combustor from P1 and S1 two-stage injector stations, each stage has four injectors at the top and bottom that equally spaced with spacing of 25.4 mm. The diameters of the two stages of injectors are 3.1750 mm and 2.3876 mm with inclination angles of 15° and 90° respectively. For more details on the combustor configuration, the experimental set-up and data measurements please refer to the relevant references [7, 8, 36, 37]. Due to the symmetry of combustor structure, one quarter of the rig geometry with symmetry boundary conditions is used for present simulation to reduce the computational cost [7]. Referring to the mesh resolution of Storch *et al.* [7] and the mesh independence analysis in Part 2 of *Supplementary material*, a hexahedral structured mesh consisting of about 1.40 million mesh cells is finally adopted to discretize the computational domain. Figure 2(c) demonstrates the mesh distribution near the two-stage fuel jets and the cavity, injectors adopt outer and inner "O" grid block schemes, and mesh cells are clustered near the fuel jets, shear layers of cavity, and walls.

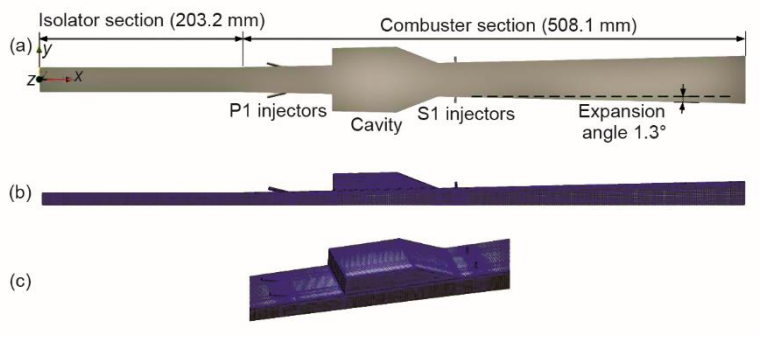

Figure 2. (a) The geometry schematic of the HIFiRE-2 scramjet combustor [mm], (b) the computational mesh of one quarter of the rig geometry, and (c) mesh refinement around two-stage fuel jet and cavity

The boundary conditions and experimental data used in the present combustion simulation are determined based on the ground experiment [36] and the accompanying simulation study [7]. The results of flight Mach numbers, Ma_∞, of 5.84 and 6.50 are taken as examples to illustrate the applicability of the preferred reduced mechanism. The flow paramaters of combustor inlet and equivalence ratios of two stages (Φ_P and Φ_S) are summarized in tab. 1. As the experiments are conducted in arc-heated tunnel, no contaminant component introduced in free incoming air flow. The mass-flow rate of methane/ethylene duel fuel for each stage is determined by the mass-flow rate of the air-flow and the corresponding equivalence ratios, and the total temperature of fuel is 300 K. The turbulent intensity, I, of air-flow and fuel jets are both taken as 5%. The turbulent kinetic energy, k, and specific dissipation rate, ω, are, respectively, estimated by $1.5(UI)^2$ and $k^{0.5}/(C_\mu^{0.25}l)$, where U is the magnitude of velocity and constant C_μ equals to 0.09. Turbulent length scale, l, is calculated by $0.07L$, where the characteristic scale, L, are the diameter of fuel injectors and the hydraulic diameter for combustor inlet. Wall functions of kqRWallFunction, omegaWallFunction, alphatWallFunction, and nutkWallFunction are adopted and targeted for high Reynolds number flow to model corresponding turbulence variables in boundary layers.

Table 1. The boundary conditions of two experimental conditions with flight Mach numbers of 5.84 and 6.50

Ma_∞	T_0 [K]	T [K]	p_0 [MPa]	p [MPa]	U [ms^{-1}]	Φ_t	Φ_P	Φ_S
5.84	1550	751.53	1.482	80.00	1365.71	0.65	0.15	0.50
6.50	1848	895.19	1.496	74.50	1510.84	1.00	0.40	0.60

Numerical simulation set-up

The combustion simulations are performed using the high speed gas phase compressible combustion solver [38] developed on the open-source platform OpenFOAM [39]. The inviscid convective fluxes are evaluated by Kurganov and Tadmor scheme [40, 41]. Second-order Crank-Nicholson time integration scheme is used [42]. Second-order total variation decreasing scheme, van Leer flux limiter [43], is used for divergence schemes of velocity, species mass fraction, internal energy, and turbulence variable fluxes. Laplacian schemes are Gauss linear corrected and the surface normal gradient scheme is corrected. The gradient schemes of turbulence variables, velocity, and pressure are cellLimited Gauss Linear 1, and the others are Gauss

linear by default. The interpolation scheme for the reconstructed density, velocity, temperature, and species mass fraction is van Leer and the others are linear by default. Ignition in simulation is accomplished by means of adding energy source terms in the patch region over a period. Adjustable time step is used and the maximum Courant-Friedrichs-Lewy number is set to 0.3. turbulent Schmidt number and turbulent Prandtl numbers are, respectively, set to 0.9 and 0.72. The SST k-ω turbulence model [44-46] and the partially stirred reactor (PaSR) combustion model [47-49] are respectively used to model turbulent flow, turbulence and combustion interaction. The model constant, C_{mix}, in PaSR is taken as 0.01 [50, 51]. The mechanism reduction method for TDAC part is EFA reduction method [25, 52] and ISAT algorithm [53]. On the TDAC reduction, the ISAT tabulation tolerance, $\varepsilon_{\mathrm{ISAT}}$, and the reduction tolerance, $\varepsilon_{\mathrm{EFA}}$, are both set to 1×10^{-4} according to previous related studies [24-26]. Previous studies indicated that thermal radiation can affect the combustion characteristics of premixed combustible mixtures in 1-D laminar burning velocity [54, 55]. Whereas the radiation effect is usually ignored in the combustion simulations in engineering scale combustor of HIFiRE-2 scramjet [7, 32, 33, 56], hence the effect is not considered in the current simulations.

Results and discussions

Acquisition of preferred reduced mechanism and its systematic kinetic verifications

Following the scheduled reduction strategy in fig. 1, the skeletal reduction is carried out for NUIGMech1.2 by setting the maximum relative error (MaxRE) of IDT ≤ 20% [57] under the target reduction conditions.The reduced mechanisms of the surrogate fuel obtained at different stages are summarized in tab. 2. After the first stage of species elimination using PFAEP method [19], the obtained reduced mechanism 78S-472R is significantly reduced compared to the preprocessed mechanism 581S-3200R. A more compact reduced mechanism 34S-208R is derived in the second stage reduction for uncertain species set by adopting the improved SA method [20] with a slight increase in the mean relative error (MeanRE) of IDT from 3.83% to 7.44%. After reaction elimination based on the method of CSP importance index [21], the reduced mechanism 34S-181R is obtained with the MeanRE of 8.02%. Given its compact size and the ability to predict IDT within reasonable accuracy [57], the mechanism 34S-181R is assumed as the preferred reduced mechanism for the surrogate fuel. Due to the absence of kinetic experiments for the compositions of current surrogate fuel, the kinetic performance for its reduced mechanism 34S-181R are validated for methane and ethylene separately under conditions relevant to the reduction conditions. Furthermore, considering the mechanisms applicable for dual fuel of methane and ethylene, such as mechanisms of Sharma *et al.* (50S-373R) [29], Xue *et al.* (149S-925R) [19], Luo *et al.* (44S-269R) [31], and GRI-Mech 3.0 (53S-325R)

Table 2. Dual fuel reduced mechanisms obtained at different static reduction stages

Reduction method	Reduced mechanisms[a]	MaxRE [b]	MeanRE [b]
Extraction and clean-up	581S-3200R	–	–
PFAEP	78S-472R	13.70%	3.83%
PFAEP + improved SA	34S-208R	18.54%	7.44%
PFAEP + Improved SA + CSP importance index	34S-181R	19.64%	8.02%

[a] Labeled by the number of species and reactions in the corresponding reduced mechanism.
[b] Maximum relative error and mean relative error under the reduction conditions.

[13], their kinetic performances are systematically compared with the preferred skeletal mechanism obtained in present work in the *Supplementary material*. Compared to these mechanisms, the preferred skeletal mechanism not only presents favorable prediction results, but also more compact in size. Thus, it is more suitable for combustion simulations of HIFiRE-2 combustor fueled by the surrogate fuel.

Since auto-ignition of fuel has been proved to be responsible for the flame stabilization mechanism in combustion simulations of scramjet combustors [58, 59], the capability of the reduced mechanism on the IDT of fuel/air mixtures is first verified. Hu *et al.* [60] conducted the experimental measurements of IDT for methane/air mixture in a shock tube under wide temperature range, pressure of 1 and 3 atmosphere, and equivalence ratio, Φ, of 0.5, 1.0, and 2.0. Yang *et al.* [57] supplemented the experimental measurements of IDT for ethylene/air mixtures in a shock tube under wide temperature range, pressure of 1 and 4 atmosphere, and Φ of 0.5, 1.0, and 2.0. Figures 3 and 4, respectively, show the comparison of the prediction results of IDT of the reduced mechanism 34S-181R and the detailed mechanism NUIGMech1.2 for methane/air and ethylene/air mixture with different equivalent ratios under corresponding conditions. In the figures, symbols are experimental data, solid lines are prediction results using the reduced mechanism, and the dashed lines are prediction results using the original detailed mechanism NUIGMech 1.2. This default rule is followed subsequently unless otherwise stated. As can be observed, the reduced mechanism with significantly reduced size can still well reproduce the simulation results of the detailed mechanism under various conditions, and its simulation results are in good agreement with experimental data.

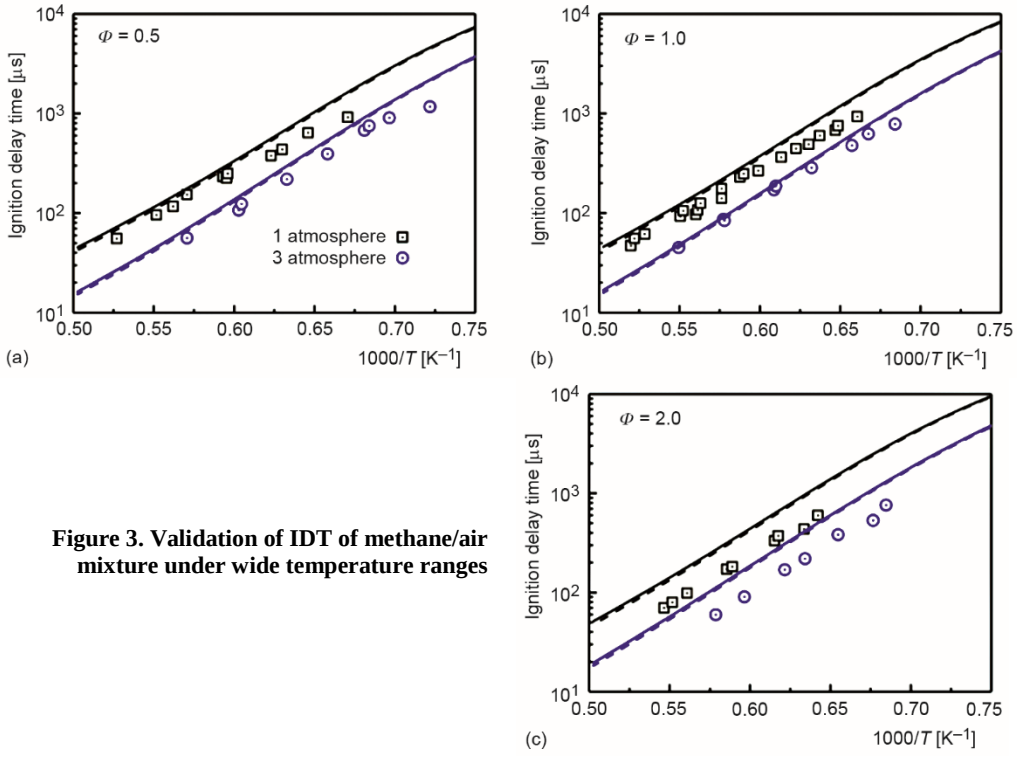

Figure 3. Validation of IDT of methane/air mixture under wide temperature ranges

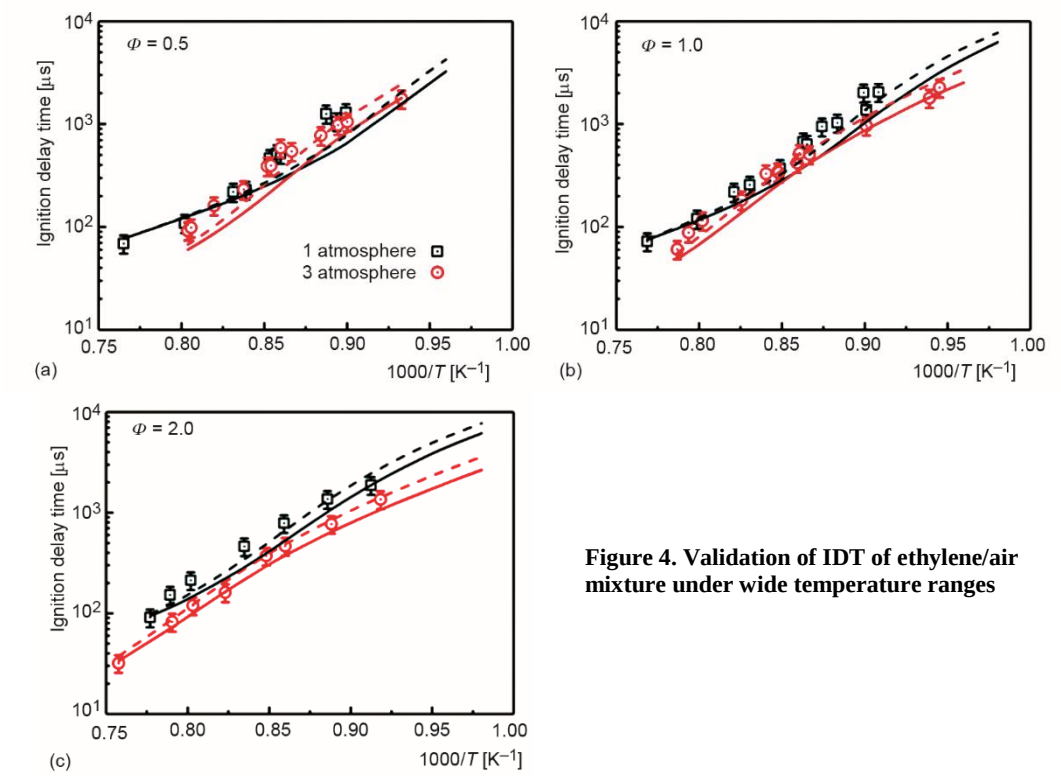

Figure 4. Validation of IDT of ethylene/air mixture under wide temperature ranges

As the residence time of the fluid in recirculation zones formed by the flame stabilizer is significantly longer and the flow velocity is lower, the accurate prediction of LFS becomes relevant under this scenario [61]. Figures 5 and 6, respectively, depict the comparison of the prediction results of the reduced and detailed mechanisms for LFS of methane/air and ethylene/air mixtures with various equivalence ratios at different initial pressures and temperatures. As can be observed the reduced mechanism can accurately capture the change of LFS with initial pressure and temperature, and its simulation results coincide well with the experimental data of methane/air [60, 62-64] and ethylene/air [65-70] mixtures provided by different researchers.

The SCP obtained in a jet-stirred reactor (JSR) are able to effectively characterize the evolution for consumption and production of concerned species under investigated operating conditions. Cong and Dagaut [71] performed JSR experiments for methane oxidation under different conditions (T = 900-1450 K, p = 1.0 atmosphere, and Φ = 0.1, 0.6, and 1.5) using N_2 diluted methane with an initial mole fraction of 0.01 and a residence time of 120 ms. Jallais *et al.* [72] performed JSR experiments for ethylene oxidation under different conditions (T = 773-900 K, p = 1.0 atmosphere, and Φ = 3, 5, and 10) using N_2 diluted ethylene with an initial molar fraction of 0.05 and a residence time of 1.3 seconds. In comparison with the corresponding experimental data [71, 72], figs. 7 and 8 successively illustrate the simulated concentration profiles using the reduced and detailed mechanisms for fuel (CH_4 and C_2H_4) and major products (CO, CO_2, *etc.*) during oxidation of $CH_4/O_2/N_2$ mixture and $C_2H_4/O_2/N_2$ mixture with different equivalence ratios. From the comparison results, one can conclude that the reduced mechanism has a favorable prediction performance on fuel consumption and major product generation.

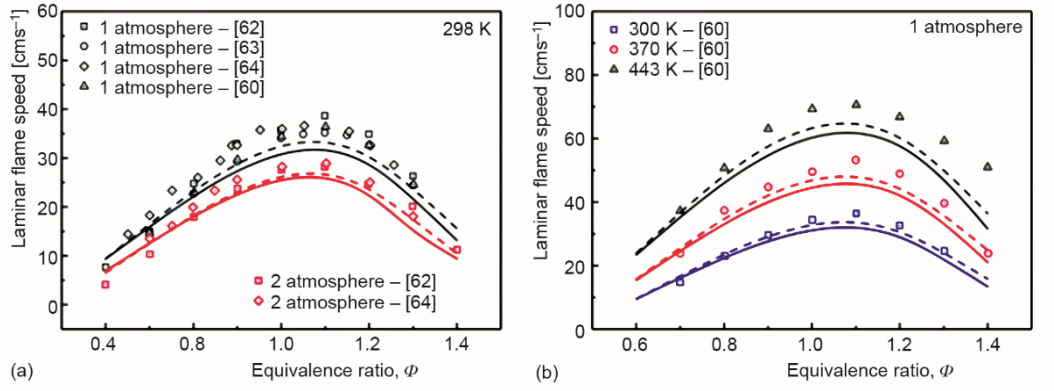

Figure 5. Validation of LFS of methane/air mixture under wide equivalence ratio ranges

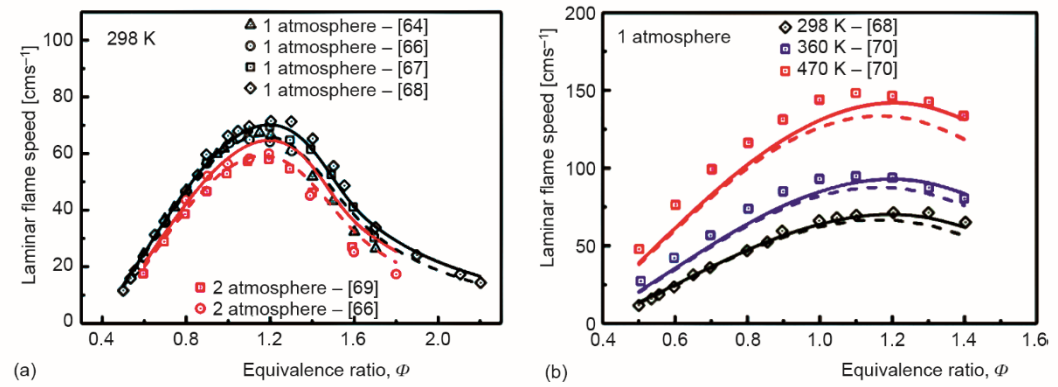

Figure 6. Validation of LFS of ethylene/air mixture under wide equivalence ratio ranges

When analyzing premixed flames, AFTP are critical for characterizing stable combustion region [73, 74]. Figure 9 provides the comparison of AFTP for the reduced and detailed mechanisms under initial temperature of 1200 K, pressure of 3 atmosphere, and equivalence ratios ranging from 0.1-4.0. In following figures, symbols are prediction results using the original detailed mechanism NUIGMech 1.2, and solid lines are prediction results using the reduced mechanism. For simulation settings, the initial temperature is determined by the non-reacting temperature field with fuel injected around the two cavities, the pressure is determined by the combusor experimental pressure [7] for the two operating conditions in tab. 1, the fuel and oxidizer are respectively set to be surrogate fuel and air. The AFTP simulated with the two mechanisms are visually indistinguishable, which demonstrates the reliability of the predicted results for the thermochemical properties of the reduced mechanism.

The “S”-curves characterize the evolution of combustion state of premixed mixture in perfectly stirred reactor with residence time [50, 75]. Figure 10 illustrates the comparison of “S”-curves simulated by the reduced and detailed mechanism for initial temperature of 1200 K, pressure of 3 atmosphere, and equivalence ratios of 0.5-1.5. The initial temperature, fuel and oxidizer in simulation set-up are consistent with the aforementioned description. As can be observed, the reduced mechanism well maintain the prediction performance of the detailed mechanism on the combustion states of ignition, extinction, intermediate unstable combustion, and stable combustion of premixed mixtures.

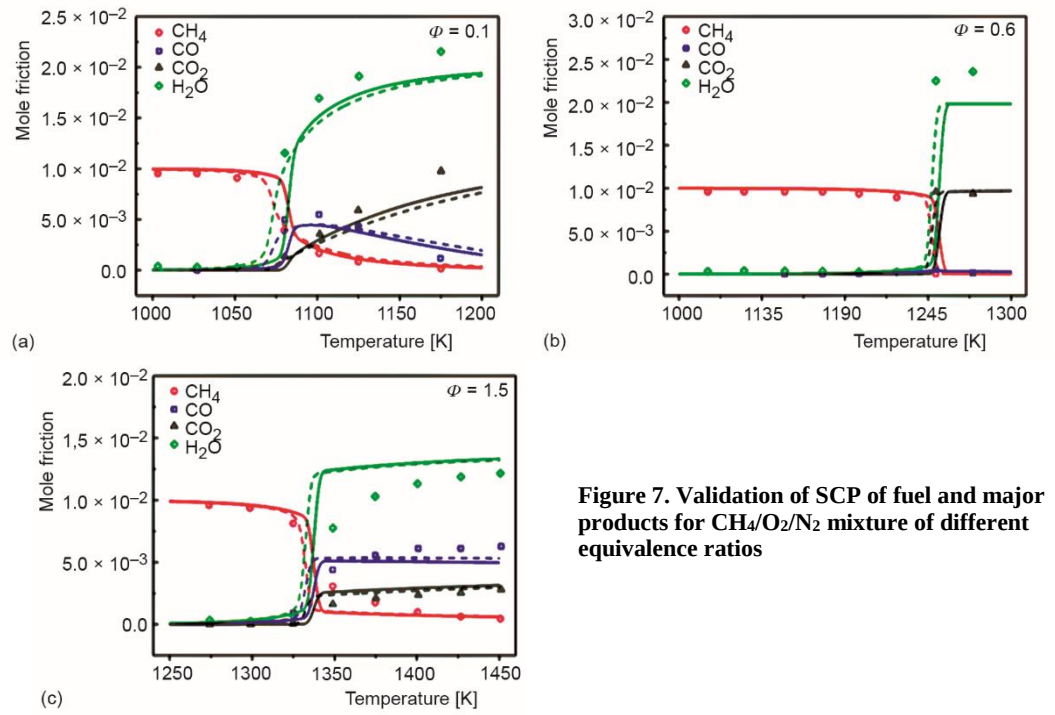

Figure 7. Validation of SCP of fuel and major products for $CH_4/O_2/N_2$ mixture of different equivalence ratios

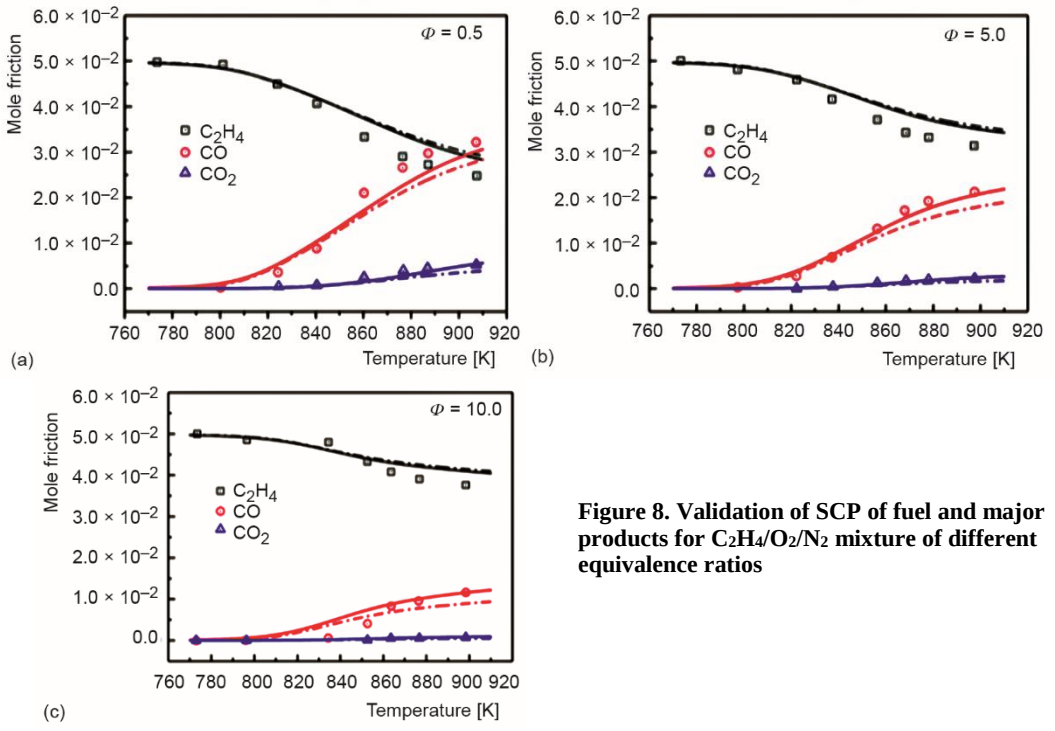

Figure 8. Validation of SCP of fuel and major products for $C_2H_4/O_2/N_2$ mixture of different equivalence ratios

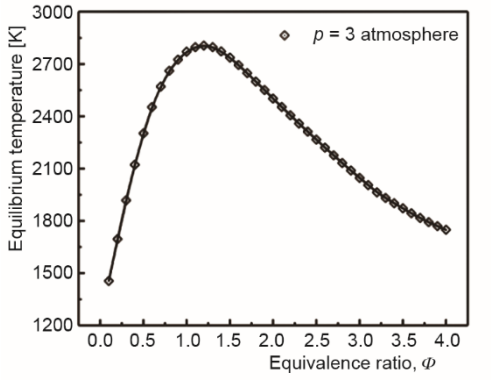

Figure 9. Validation of AFTP of surrogate fuel/air mixture of different equivalence ratios under initial temperature of 1200 K and pressure of 3 atmosphere

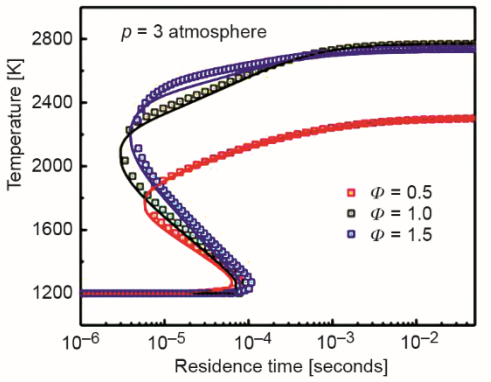

Figure 10. Validation of "S"-curves of surrogate fuel/air simulated by different mechanisms at equivalence ratios of 0.5-1.5 and pressures of 3 atmosphere

According to previous systematic kinetic verifications, the simulation results of the reduced mechanism match well with corresponding experimental measurements for IDT, LFS, and SCP. Meanwhile, it provides consistent results with the detailed mechanism in aspect of AFTP and "S"-curves. Reaction path analyses of the detailed mechanism and the reduced mechanism for the ignition moments relevant to combustion conditions are provided in *Supplementary material*. As can be concluded from the analysis results, the preferred reduced mechanism retains dominant key reaction pathways of the surrogate fuel in combustion processes. The results demonstrate that this compact and high-fidelity reduced mechanism for the surrogate fuel is well prepared for the combustion simulations of scramjet combustor in next section. This mechanism can be acquired from the *Supplementary material*.

Application of the reduced mechanism for surrogate fuel in combustion simulations

The reduced mechanism 34S-181R of surrogate fuel obtained by the static integrated reduction method is applied to combustion simulations of HIFiRE-2 combustor. The TDAC method of dynamic EFA [25] reduction method and the ISAT algorithm [53] is also adopted for further ru*n*-time speed-up.

The static pressure distribution profiles obtained from simulations of the two operating conditions in tab. 1 are compared with the corresponding experimental measurements [36]. Numerical schlieren images (calculated by $|\nabla\rho|$) for cold and hot states are synchronously provided, due to the flow field shock wave structure can significantly affect the pressure distribution profiles.

Static pressure profiles and numerical schlieren images of cold and hot states for $Ma_\infty = 5.84$ and $Ma_\infty = 6.50$ are sequentially presented in figs. 11 and 12. As for the cold states, the flow structures in the whole combustor are well captured in schlieren images. Expansion waves formed at starting point of the divergence angle of combustor and their reflected waves are observed upstream of the combustor. Besides, the expansion waves formed at the shear layers of the two cavities are firstly reflected between the shear layers, and then reflected several times on the upper and lower walls downstream of the combustor. As for the

pressure profiles, the pressure begins to drop at the starting point of upper cavity and maintains essentially uniformity within the cavity, the pressure gradually rises as the shear layer of the cavity impinges the trailing edge of the cavity, and the pressure rises further due to the narrowing of the flow path along the trailing edge of the cavity. According to the flow phenomena in the combustor resolved from numerical schlieren images, the distribution characteristics of the pressure profiles at the downstream of combustor upper wall can be interpreted intuitively. As for the hot states, the simulated pressure profiles agree well with the corresponding experimental measurements in terms of the initial pressure rise position and the pressure rise ratio. The agreement means current simulations resolve well the combustion intensity and distribution of heat release that can be reflected by the static pressure profiles along the combustor [76]. Due to the thermal blockage caused by the combustion occurred in cavities and the narrowed flow path, there are complex interactions between flow and combustion near the aftwall of the cavities, resulting in some differences between the simulation results and the experimental measurements. As can be noted in schlieren images, pre-combustion shock waves caused by combustion heat release propagate to upstream of the combustor. As combustion occurs in cavities, shock waves undergo multiple reflections between cavity shear layers. At the divergence section downstream of cavities, the intensity of the reflected shock waves gradually decreases, which is well reflected in the upper wall pressure profile distribution. Additionally, due to the lower global equivalence ratio of the first stage fuel injection for the case $Ma_\infty = 5.84$, the intensity of the upstream pre-combustion shock waves is higher compared to that of $Ma_\infty = 6.50$. The wall pressure of the latter is higher near the first stage fuel injection due to higher global equivalence ratio.

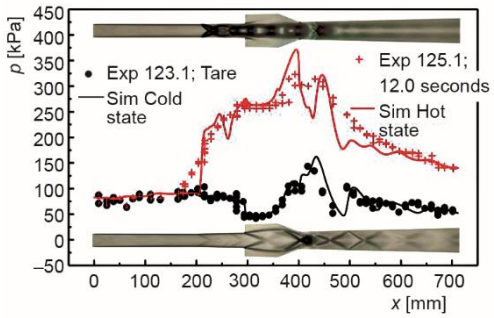

Figure 11. Static pressure profiles and numerical schlieren images of cold and hot states for flight Mach number of 5.84

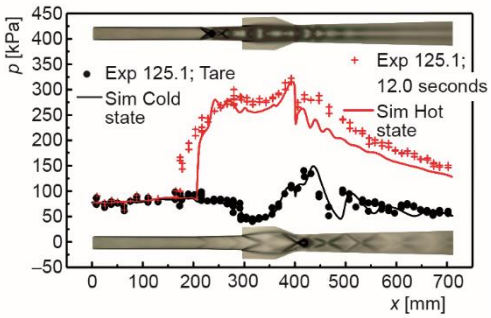

Figure 12. Static pressure profiles and numerical schlieren images of cold and hot states for flight Mach number of 6.50

Conclusions

Taking the surrogate fuel of partially cracked JP-7 fuel, *i.e.*, 64% ethylene and 36% methane, utilized in the HIFiRE-2 scramjet combustor as an example, present work systematically explores the workflow of integrated reduction, comprehensive kinetic validations of obtained reduced mechanism, and the application of the reduced mechanism to combustion simulation. Under the target reduction conditions for temperature range of 900-1800 K, pressure range of 1-4 atmosphere, and equivalence ratio range of 0.25-5.0, a preferred reduced mechanism (34 species and 181 reactions) of the surrogate fuel with remarkably reduced size is obtained by the proposed static integrated reduction strategy, which successively consists methods

of PFAEP, improved SA and CSP importance index. In comprehensive kinetic validations, this reduced mechanism presents favorable performance in terms of IDT, LFS, SCP, AFTP and "S"-curves, which demonstrates the reliability of the mechanism derivated from the integrated reduction strategy. The applicability of this high-fidelity mechanism is illustrated in combustion simulations for HIFiRE-2 scramjet combustor under two operating conditions with simulated flight Mach numbers of 5.84 and 6.50 combining with TDAC of EFA dynamic reduction method and ISAT algorithm for further ru*n*-time speed-up. Based on simulation results, the flow and combustion characteristics in the combustor are investigated jointly for the two cases. The integrated reduction strategy and systematic kinetic verification method used in present work provides reference values for the application of more complex surrogate fuel mechanisms in scramjet combustor simulations.

Acknowledgment

This work is supported by the Science & Technology Department of Sichuan Province award (No. 2023NSFSC0058) and the project of WDZC6142703202201.

Nomenclature

C_{mix} – mixing constant of PaSR model
I – turbulent intensity
k – turbulent kinetic energy, [m^2s^{-2}]
L – characteristic scale, [m]
l – turbulent length scale, [m]
Ma_∞ – flight Mach number
p_0 – total pressure, [MPa]
p – static pressure, [kPa] or [atm]
T_0 – total temperature, [K]
T – static temperature, [K]
U – magnitude of velocity, [ms^{-1}]

Greek symbols

ε – tolerance
ρ – density, [kgm^{-3}]
Φ – equivalence ratio
ω – specific dissipation rate, [$1s^{-1}$]

Subscripts

EFA – indication of elementary flux analysis method
ISAT – indication of ISAT algorithm
P – variable at P1 injector station
S – variable at S1 injector station
t – total sum of variable

Acronyms

AFTP – adiabatic flame temperature profiles
CSP – computational singular perturbation
DAC – dynamic adaptive chemistry
EFA – elementary flux analysis
HIFiRE-2 – hypersonic international flight research experimentation flight 2
IDT – ignition delay times
ISAT – i*n*-situ adaptive tabulation
LFS – laminar flame speeds
MaxRE – maximum relative error
MeanRE – mean relative error
PaSR – partially stirred reactor
PFAEP – path flux analysis with error propagation
SA – sensitivity analysis
SCP – species concentration profiles
TDAC – tabulation of dynamic adaptive chemistry

Supplementary material

Comparisons on kinetic performance for mechanisms of methane and ethylene

Considering the mechanisms applicable for dual fuel of methane and ethylene in literature review in introduction section such as mechanisms of Sharma *et al.* (50S-373R) [29], Xue *et al.* (149S-925R) [19], Luo *et al.* (44S-269R) [31], and GRI-Mech 3.0 (53S-325R) [13], their kinetic performances are systematically compared with the preferred skeletal mechanism

(34S-181R) obtained in present work. Under relevant conditions as involved for comparisons for the detailed mechanism and preferred skeletal mechanism, the systematic comparisons on ignition delay times (IDT), laminar flame speeds (LFS), and species concentration profiles (SCP) for different mechanisms are respectively performed for methane and ethylene.

Figures S1 and S2, respectively, depict the comparisons of IDT for methane/air mixture and ethylene/air mixture predicted by the five mechanisms under wide working conditions. As for the predictions of IDT for methane/air mixture, All the five mechanisms present good performance in terms of IDT for methane/air mixture. Among them, GRI-Mech 3.0 [13] is a detailed mechanism mainly optimized for natural gas combustion. The present skeletal mechanism presents well consistent with that of Xue *et al.* [19]. The skeletal mechanisms of Sharma *et al.* [29] and Luo *et al.* [31] are basically identical, as they are both reduced from the high temperature detailed mechanism USC Mech-II [11] and retain the key species and reactions that dominate ignition processes. As for the predictions of IDT for ethylene/air mixture, the mechanism of Sharma *et al.* [29] deviates significantly from the corresponding experimental measurements under all investigated working conditions. The GRI-Mech 3.0 [13] has barely satisfactory simulation results at $p = 1$ atmosphere and presents significant prediction deviations at $p = 4$ atmosphere, which indicates that it fails to capture pressure effect on ignitions. The mechanism of Luo *et al.* [31] predicts poorly under fuel-lean working conditions ($p = 1$, 4 atmosphere, $\Phi = 0.5$). The skeletal mechanism obtained by this work and that of Xue *et al.* [19] offer favorable predictions for all working conditions.

Figures S7 and S8 successively present the comparisons of SCP of fuel (CH_4 and C_2H_4) and major products (CO, CO_2, *etc.*) predicted by different mechanisms for $CH_4/O_2/N_2$ mixture and $C_2H_4/O_2/N_2$ mixture of different equivalence ratios at 1 atmosphere. For the predictions of species concentration during the oxidation of $CH_4/O_2/N_2$ mixtures, GRI-Mech 3.0 [13] is unable to yield correct evolution profiles of species concentration with respect to temperature. The skeletal mechanisms of Sharma *et al.* [29] and Luo *et al.* [31] present essentially identical predictions, but both misestimate the location of the temperature for rapid initiation of reactions. For very lean combustion conditions ($\Phi = 0.1$), the predictive performance of the skeletal mechanism of Xue *et al.* [19] is also poor. Whereas it is evident that only the skeletal mechanism obtained in present work is competent for the prediction of species concentration profiles for all investigated working conditions for $CH_4/O_2/N_2$ mixture. As for the prediction of species concentration during the oxidation of $C_2H_4/O_2/N_2$ mixture, GRI-Mech 3.0 [13] even can not predict the reaction occurrence under the corresponding investigated working conditions, the skeletal mechanism of Luo *et al.* [31] yields predictions that significantly deviate from the experimental data, and the skeletal mechanism of Sharma *et al.* [29] again misestimate the location of the temperature for rapid initiation of reactions. The predictive performance of the skeletal mechanism obtained in present work and that of Xue *et al.* [19] are relatively superior, and the former being in better agreement with experimental data.

Figures S3 and S4 provide the comparisons of LFS for methane/air mixture and ethylene/air mixture predicted by different mechanisms under initial temperature of 298 K and pressures of 1 and 2 atmosphere. Except for GRI-Mech 3.0 [13], other mechanisms can well describe the LFS for both methane/air mixture and ethylene/air mixture under investigated conditions, and their simulation results also reproduce well the effect of different equivalence ratios and pressures on the flame propagation characteristics. Figures S5 and S6 illustrate the comparisons of LFS for methane/air mixture and ethylene/air mixture of different equivalence ratios predicted by different mechanisms under pressure of 1 atmosphere with three different initial

temperatures. Apart from GRI-Mech 3.0 [13], other mechanisms match well with corresponding experimental data, and can correctly predict the variation of laminar flame speed with different initial temperatures. As mentioned earlier, GRI-Mech 3.0 is primarily geared towards the combustion of natural gas, and it is not well-suited for ethylene combustion.

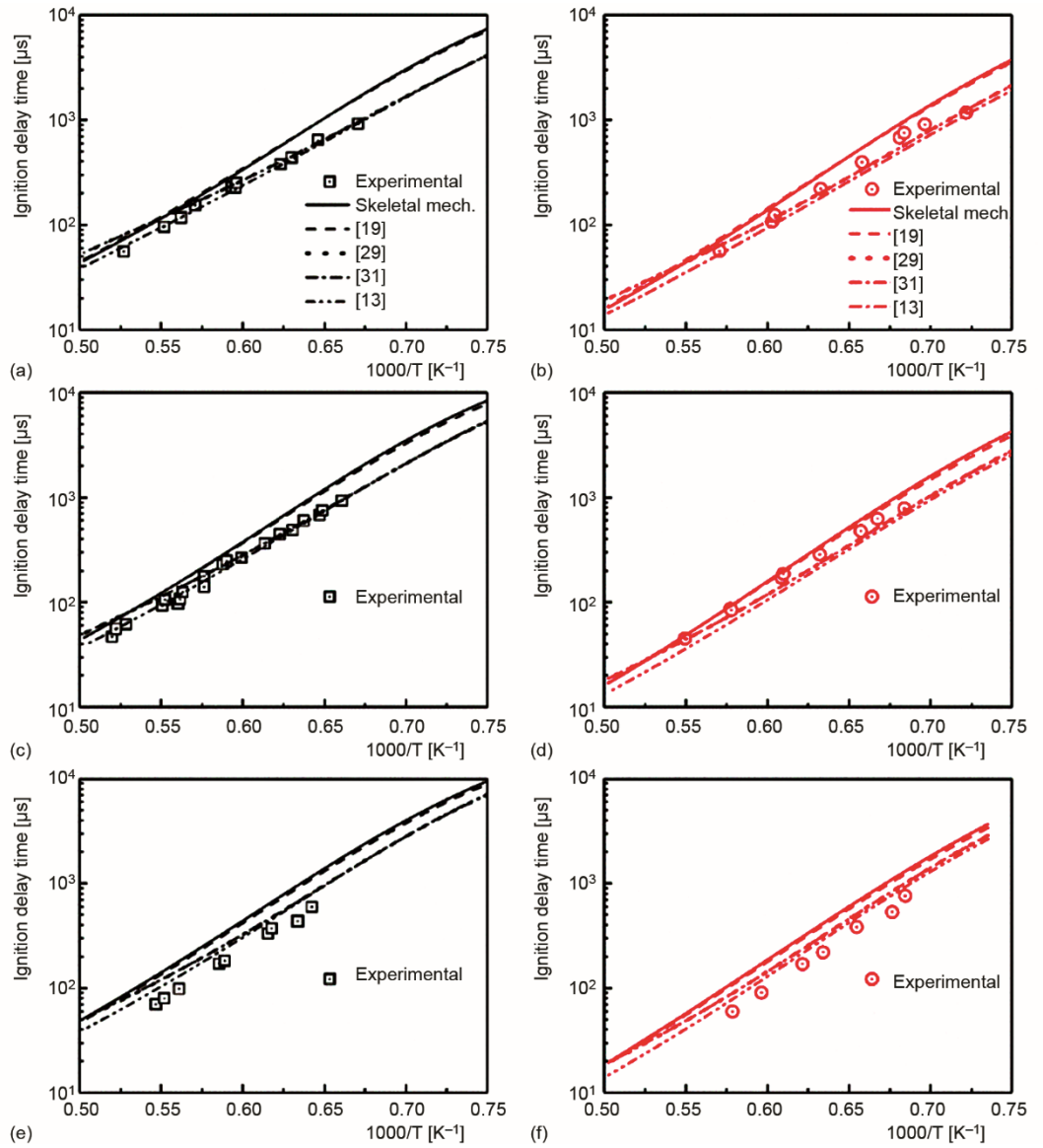

Figure S1. The IDT for methane/air mixture predicted by different mechanisms under wide temperature range, pressures of 1 and 3 atmosphere, equivalence ratios of 0.5, 1.0, and 2.0; (a) p = 1 atmosphere, Φ = 0.5, (b) p = 3 atmosphere, Φ = 0.5, (c) p = 1 atmosphere, Φ = 1.0, (d) p = 3 atmosphere, Φ = 1.0, (e) p = 1 atmosphere, Φ = 2.0, and (f) p = 3 atmosphere, Φ = 2.0

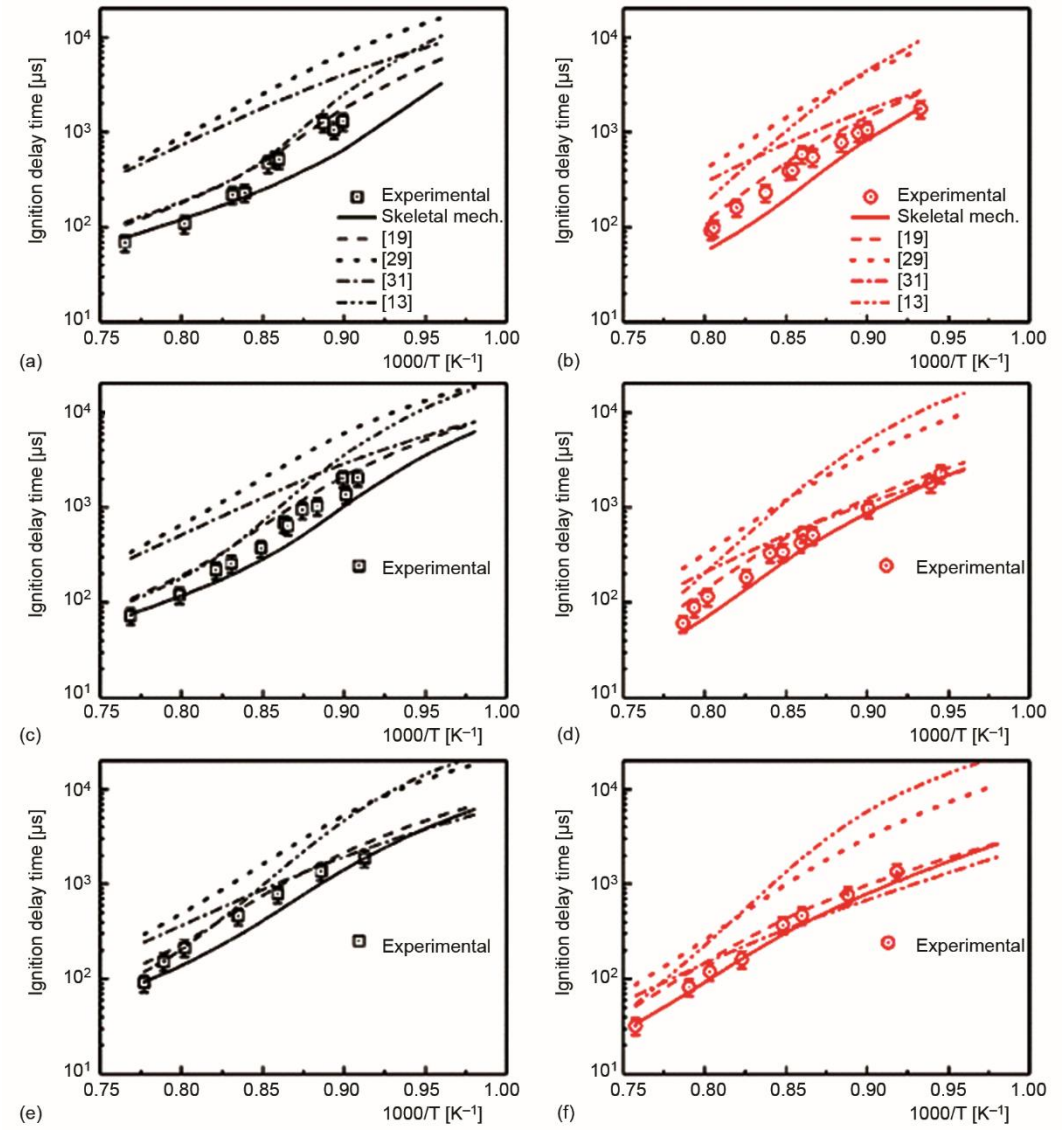

Figure S2. The IDT for ethylene/air mixture predicted by different mechanisms under wide temperature range, pressures of 1 and 4 atmosphere, equivalence ratios of 0.5, 1.0, and 2.0; (a) p = 1 atmosphere, Φ = 0.5, (b) p = 4 atmosphere, Φ = 0.5, (c) p = 1 atmosphere, Φ = 1.0, (d) p = 4 atmosphere, Φ = 1.0, (e) p = 1 atmosphere, Φ = 2.0, and (f) p = 4 atmosphere, Φ = 2.0

By comparing the kinetic performances of the preferred skeletal mechanism with those of related mechanisms of methane and ethylene in the literature review under the relevant combustion conditions, the favorable performance of this reduced skeletal mechanism is further proven in the detailed comparative results and discussions. This is because more new reaction pathways and updated reaction rates related to methane and ethylene combustion are included in the newly developed detailed mechanism NUIGMech1.2 [14] compared to GRI-Mech 3.0 [13], USC Mech-II [11] and AramcoMech 3.0 [30], and they are retained in present reduced

skeletal mechanism. Furthermore, the present reduced skeletal mechanism has an advantage in terms of mechanism size compared to the other mechanisms. Thus, it is more suitable for combustion simulations of the surrogate fuel.

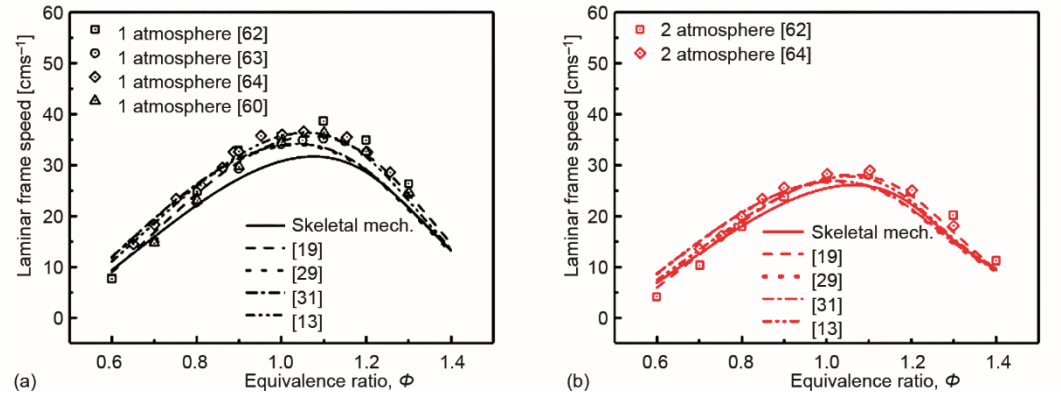

Figure S3. The LFS for methane/air mixture predicted by different mechanisms under initial temperature 298 K, pressures of 1 and 2 atmosphere; (a) p = 1 atmosphere, T = 298 K and (b) p = 2 atmosphere, T = 298 K

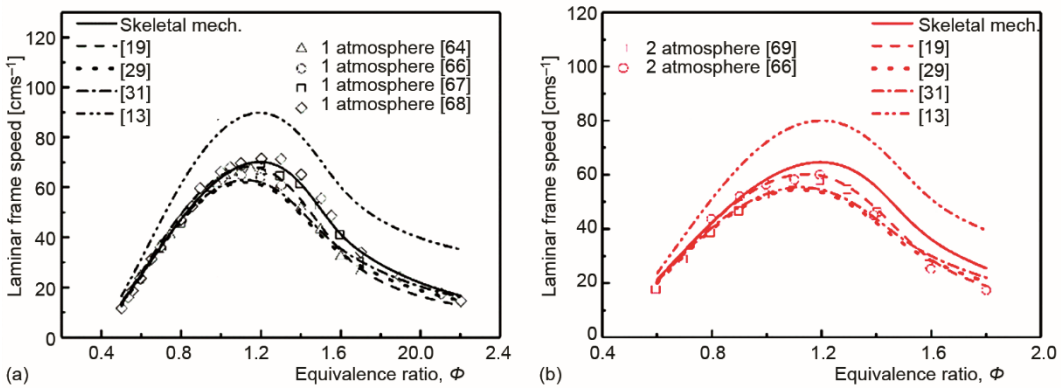

Figure S4. The LFS for ethylene/air mixture predicted by different mechanisms under initial temperature 298 K, pressures of 1 and 2 atmosphere; (a) p = 1 atmosphere, T = 298 K and (b) p = 2 atmosphere, T = 298 K

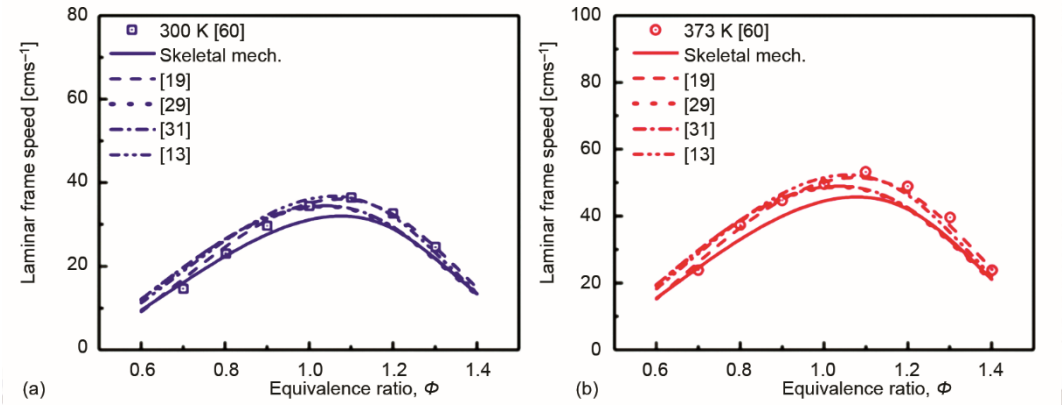

Fig. S5. The LFS for methane/air mixture predicted by different mechanisms under pressure of 1 atmosphere, initial temperature of 300 K, 373 K, and 443 K; (a) p = 1 atmosphere, T = 300 K and (b) p = 2 atmosphere, T = 373 K

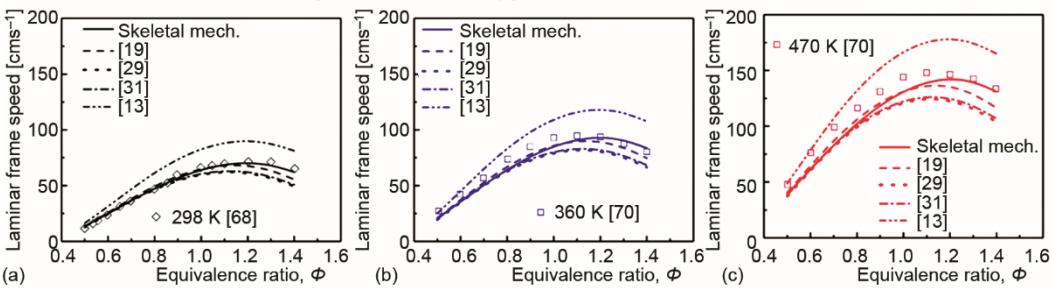

Figure S6. The LFS for ethylene/air mixture predicted by different mechanisms under pressure of 1 atmosphere, initial temperatures of 298 K, 360 K, and 470 K; (a) p = 1 atmosphere, T = 298 K, (b) p = 1 atmosphere, T = 360 K, and (c) p = 1 atmosphere, T = 470 K

Mesh independent analysis

Mesh independent analysis is carried out based on no*n*-reactive flow field of flight condition of Mach 5.84 to choose proper mesh resolution by employing three meshes respectively consisting of 0.93, 1.40, 2.12 million cells. Figure S9 shows the influence of mesh resolution on pressure profile along the upper wall in the no*n*-reactive flow. To visualize the distribution characteristics of the pressure and shock wave structures more visually, the pressure contour and numerical schlieren image (calculated by $|\nabla\rho|$) for the central cross-section of medium mesh are given in the upper and lower parts of the figure. As can be observed, the pressure distribution profiles obtained by the three mesh are uniform in trend and are visually indistinguishable from each other, and they accurately capture the flow structures in this combustor. Considering the accuracy and computational cost, the medium mesh of 1.40 million cells is finally adopted for subsequent simulations.

Reaction path analyses for ignition moments under relevant combustion conditions

Reaction path analyses around the ignition moment of the surrogate fuel are performed under initial temperature of 1200 K, pressure of 3 atmosphere, and equivalence ratios of 0.5-

1.5 to validate whether the reduced mechanism retains the key reaction pathways. It is worth emphasizing that the working conditions investigated for the present kinetic analyses are closely relevant to the two combustion conditions of this scramjet. The normalized reaction fluxes of key reaction paths for the detailed and reduced mechanisms are successively compared in figs. S10-S12. Although some of the normalized reaction flux values change to some extent after reduction due to the elimination of some species and reactions, it is observed that the dominant key reaction paths are retained in the reduced mechanism and it can effectively characterize the reaction characteristics under the investigated working conditions.

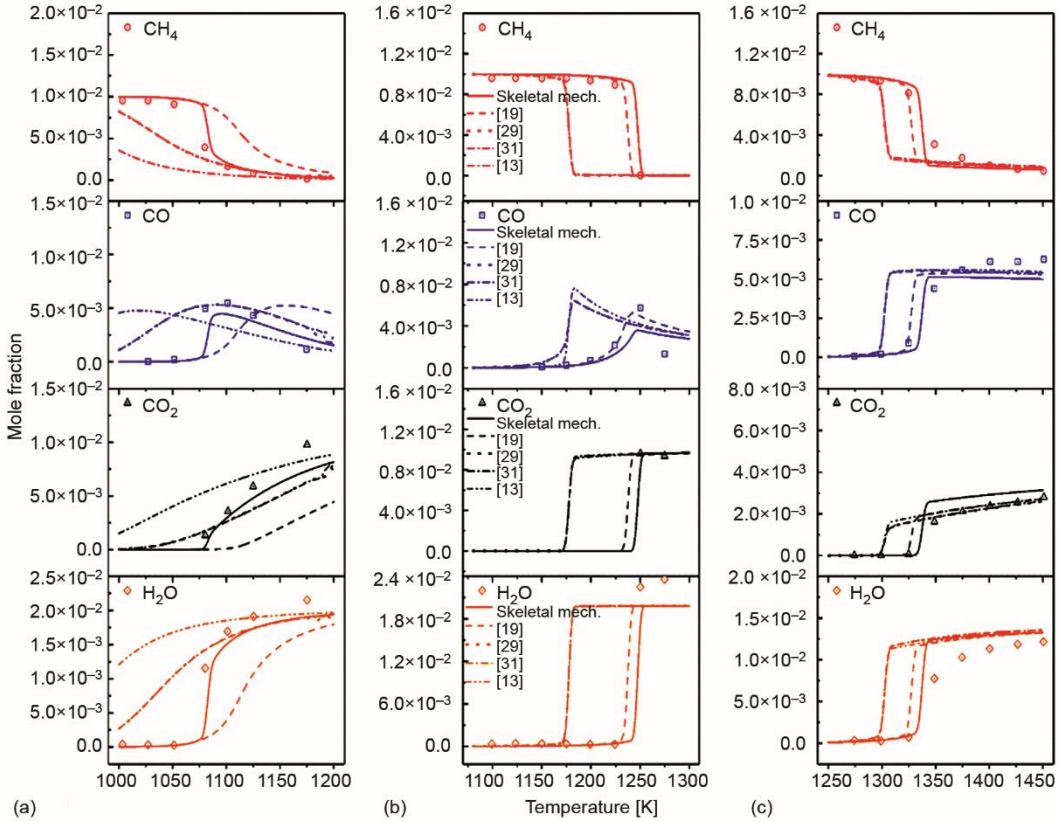

Figures S7. The SCP of fuel and major products for $CH_4/O_2/N_2$ mixture predicted by different mechanisms under 1 atmosphere, equivalence ratios of 0.1, 0.6, and 1.5; (a) Φ = 0.1, (b) Φ = 0.6, and (c) Φ = 1.5

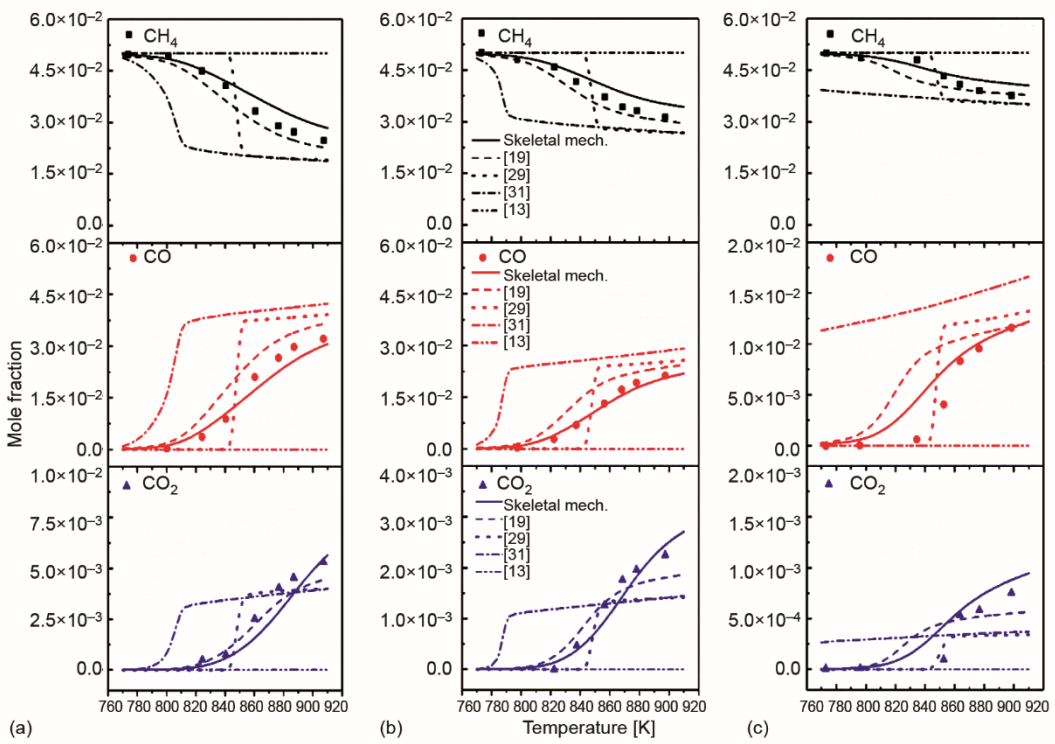

Figures S8. The SCP of fuel and major products for $C_2H_4/O_2/N_2$ mixture predicted by different mechanisms under 1 atmosphere, and equivalence ratios of 3.0, 5.0, and 10.0; (a) Φ = 3.0, (b) Φ = 5.0, and (c) Φ = 10.0

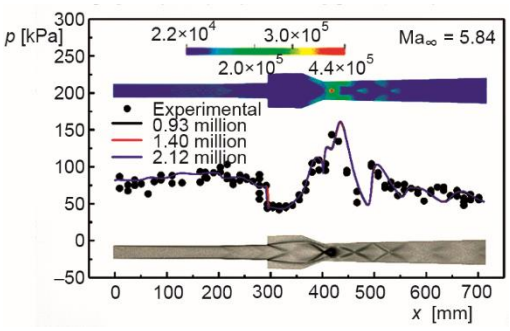

Figure S9. The influence of mesh resolution on pressure profile along the upper wall in cold flow field for flight Mach number of 5.84

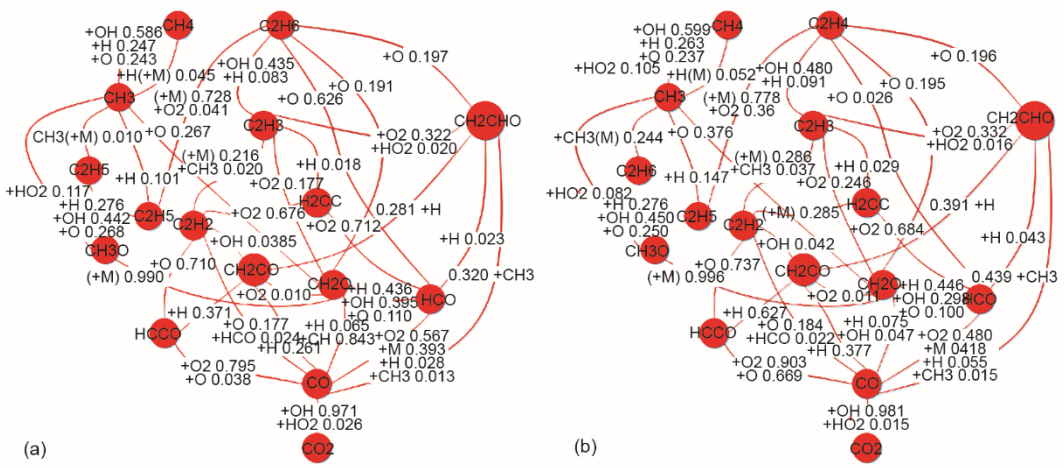

Figure S10. Reaction path analysis on ignition moment under initial temperature of 1200 K, pressure of 3.0 atmosphere, and equivalence ratio of 0.5 for the detailed (left column) and reduced (right column) mechanisms; Φ = 0.5

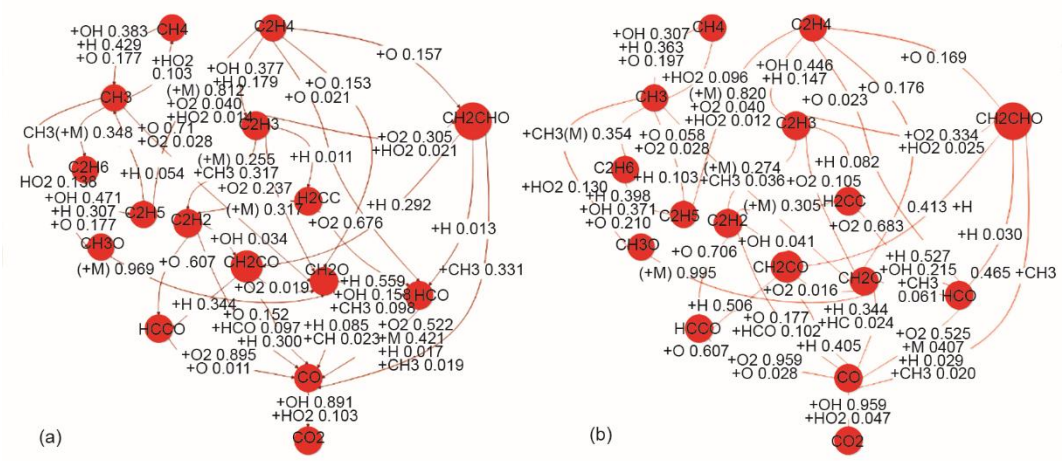

Figure S11. Reaction path analysis on ignition moment under initial temperature of 1200 K, pressure of 3.0 atmosphere, and equivalence ratio of 1.0 for the detailed (left column) and reduced (right column) mechanisms; Φ = 1.0

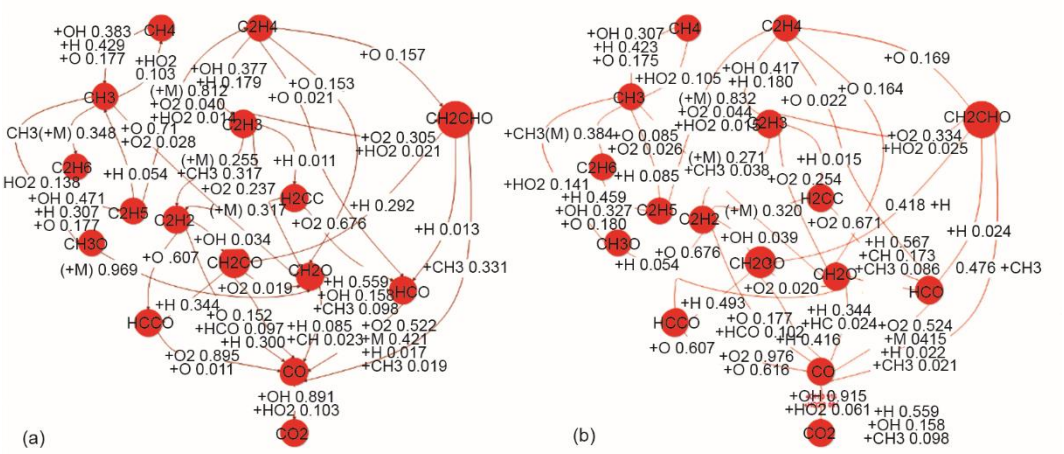

Figure S12. Reaction path analysis on ignition moment under initial temperature of 1200 K, pressure of 3.0 atmosphere, and equivalence ratio of 1.5 for the detailed (left column) and reduced (right column) mechanisms; Φ = 1.5

References

[1] Powell, O. A., *et al.*, Development of Hydrocarbon-Fueled Scramjet Engines: The Hypersonic Technology (HyTech) Program, *Journal of Propulsion and Power*, *17* (2001), 6, pp. 1170-1176
[2] Sobel, D. R., Spadaccini, L. J., Hydrocarbon Fuel Cooling Technologies for Advanced Propulsion, *Journal of Engineering for Gas Turbines and Power*, *119* (1997), 2, pp. 344-351
[3] Huang, H., *et al.*, Fuel-Cooled Thermal Management for Advanced Aeroengines, *Journal of Engineering for Gas Turbines and Power*, *126* (2004), 2, pp. 284-293
[4] Zhang, D., *et al.*, Performance Evaluation of Power Generation System with Fuel Vapor Turbine Onboard Hydrocarbon Fueled Scramjets, *Energy*, *77* (2014), Dec., pp. 732-741
[5] Zhong, F., *et al.*, Thermal Cracking and Heat Sink Capacity of Aviation Kerosene Under Supercritical Conditions, *Journal of Thermophysics and Heat Transfer*, *25* (2011), 3, pp. 450-456
[6] Spadaccini, L. J., Colket, III, M. B., Scramjet Fuels Autoignition Study, *Journal of Propulsion and Power*, *17* (2001), 2, pp. 315-323
[7] Storch, A., *et al.*, Combustor Operability and Performance Verification for HIFiRE Flight 2, *Proceedings*, 17th AIAA International Space Planes and Hypersonic Systems and Technologies Conference, San Francisco, Cal., USA, 2011
[8] Jackson, K., *et al.*, HIFiRE Flight 2 Project Overview and Status Update 2011, *Proceedings*, 17th AIAA International Space Planes and Hypersonic Systems and Technologies Conference, San Francisco, Ca., USA, 2011
[9] Pellett, G. L., *et al.* Gaseous Surrogate Hydrocarbons for a HIFiRE Scramjet that Mimic Opposed Jet Extinction Limits for Cracked JP Fuels, *Proceedings*, 55th JANNAF Propulsion Meeting, Boston, Mass, USA, 2008
[10] Wang, H., Laskin, A., A Comprehensive Kinetic Model of Ethylene and Acetylene Oxidation at High Temperatures, Progress report for an AFOSR new world vista program, Univ. of Delaware, Newark, Del., USA, 1998
[11] Wang, H., *et al.*, http://ignis.usc.edu/USC_Mech_II.htm
[12] Zhou, C.-W., *et al.*, An Experimental and Chemical Kinetic Modeling Study of 1,3-Butadiene Combustion: Ignition Delay Time and Laminar Flame Speed Measurements, *Combustion and Flame*, *197* (2018), Nov., pp. 423-438
[13] Smith, G.P., *et al.*, http://www.me.berkeley.edu/gri_mech/
[14] Martinez, S., *et al.*, A Comprehensive Experimental and Modeling Study of the Ignition Delay Time Characteristics of Ternary and Quaternary Blends of Methane, Ethane, Ethylene, and Propane Over a wide Range of Temperature, Pressure, Equivalence Ratio, and Dilution, *Combustion and Flame*, *234* (2021), 111626

[15] Baigmohammadi, M., *et al.*, A Comprehensive Experimental and Simulation Study of Ignition Delay Time Characteristics of Single Fuel C_1-C_2 Hydrocarbons over a Wide Range of Temperatures, Pressures, Equivalence Ratios, and Dilutions, *Energy & Fuels*, *34* (2020), 3, pp. 3755-3771
[16] Baigmohammadi, M., *et al.*, Comprehensive Experimental and Simulation Study of the Ignition Delay Time Characteristics of Binary Blended Methane, Ethane, and Ethylene over a Wide Range of Temperature, Pressure, Equivalence Ratio, and Dilution, *Energy & Fuels*, *34* (2020), 7, pp. 8808-8823
[17] Martinez, S., *et al.*, An Experimental and Kinetic Modeling Study of the Ignition Delay Characteristics of Binary Blends of Ethane/Propane and Ethylene/Propane in Multiple Shock Tubes and Rapid Compression Machines over a Wide Range of Temperature, Pressure, Equivalence Ratio, and Dilution, *Combustion and Flame*, *228* (2021), June, pp. 401-414
[18] Lu, T., Law, C.K., Toward Accommodating Realistic Fuel Chemistry in Large-Scale Computations, *Progress in Energy and Combustion Science*, *35* (2009), 2, pp. 192-215
[19] Xue, J., *et al.*, An Extensive Study on Skeletal Mechanism Reduction for the Oxidation of C_0–C_4 Fuels, *Combustion and Flame*, *214* (2020), Apr., pp. 184-198
[20] Xi, S., *et al.*, Reduction of Large-Size Combustion Mechanisms of *n*-Decane and *n*-Dodecane with an Improved Sensitivity Analysis Method, *Combustion and Flame*, *222* (2020), Dec., pp. 326-335
[21] Lu, T., Law, C. K., Strategies for Mechanism Reduction for Large Hydrocarbons: *n*-Heptane, *Combustion and Flame*, *154* (2008), 1, pp. 153-163
[22] Wu, K., *et al.*, Development and Fidelity Evaluation of a Skeletal Ethylene Mechanism under Scramjet-Relevant Conditions, *Energy & Fuels*, *31* (2017), 12, pp. 14296-14305
[23] Xiao, G., A Novel Integrated Strategy for Construction of a 96-Species *n*-Decane Skeletal Mechanism with Application to Ignition Delay Tester, *Energy & Fuels*, *34* (2020), 5, pp. 6367-6382
[24] Contino, F., *et al.*, Coupling of In Situ Adaptive Tabulation and Dynamic Adaptive Chemistry: An Effective Method for Solving Combustion in Engine Simulations, *Proceedings of the Combustion Institute*, *33* (2011), 2, pp. 3057-3064
[25] Li, Z., *et al.*, Assessment of O*n*-the-Fly Chemistry Reduction and Tabulation Approaches for the Simulation of Moderate or Intense Low-Oxygen Dilution Combustion, *Energy & Fuels*, *32* (2018), 10, pp. 10121-10131
[26] Wu, K., *et al.*, On the Application of Tabulated Dynamic Adaptive Chemistry in Ethylene-Fueled Supersonic Combustion, *Combustion and Flame*, *197* (2018), Nov., pp. 265-275
[27] An, J., *et al.*, Dynamic Adaptive Chemistry with Mechanisms Tabulation and In Situ Adaptive Tabulation (ISAT) for Computationally Efficient Modeling of Turbulent Combustion, *Combustion and Flame*, *206* (2019), Aug., pp. 467-475
[28] Karst, F., *et al.*, Reduction of Microkinetic Reaction Models for Reactor Optimization Exemplified for Hydrogen Production from Methane, *Chemical Engineering Journal*, *281* (2015), Dec., pp. 981-994
[29] Sharma, D., *et al.*, Development of the Reduced Chemical Kinetic Mechanism for Combustion of H_2/CO/C_1-C_4 Hydrocarbons, *Energy & Fuels*, *35* (2021), 1, pp. 718-742
[30] Zhou, C.-W., *et al.*, A Comprehensive Experimental and Modeling Study of Isobutene Oxidation, *Combustion and Flame*, *167* (2016), May, pp. 353-379
[31] Luo, Z., *et al.*, A Reduced Mechanism for Ethylene/Methane Mixtures with Excessive NO Enrichment, *Combustion and Flame*, *158* (2011), 7, pp. 1245-1254
[32] Saghafian, A., *et al.*, Large Eddy Simulations of the HIFiRE Scramjet Using a Compressible Flamelet/Progress Variable Approach, *Proceedings of the Combustion Institute*, *35* (2015), 2, pp. 2163-2172
[33] Yentsch, R. J., Gaitonde, D.V., Unsteady Three-Dimensional Mode Transition Phenomena in a Scramjet Flowpath, *Journal of Propulsion and Power*, *31* (2014), 1, pp. 104-122
[34] ***, *San Diego, CHEMKIN-PRO 15112*. 2011, Reaction design
[35] Li, S. H., *et al.*, Automatic Chemistry Mechanism Reduction on Hydrocarbon Fuel Combustion, *Chemical Journal of Chinese Universities*, *36* (2015), 8, pp. 1576-1587
[36] Hass, N. E., *et al.*, HIFiRE Direct-Connect Rig (HDCR) Phase I Ground Test Results from the NASA Langley Arc-Heated Scramjet Test Facility, *Proceedings*, 31st Airbreathing Joint Meeting, La Jolla, Cal., USA, 2010
[37] Hass, N., *et al.*, HIFiRE Direct-Connect Rig (HDCR) Phase I Scramjet Test Results from the NASA Langley Arc-Heated Scramjet Test Facility, *Proceedings*, 17th AIAA International Space Planes and Hypersonic Systems and Technologies Conference, San Francisco, Cal., USA, 2011
[38] Li, Z., *et al.*, Application of Hydrogen Mechanisms in Combustion Simulation of DLR Scramjet Combustor and Their Effect on Combustion Performance, *Fuel*, *349* (2023), 128659

[39] ***, OpenFOAM Foundation, https://openfoam.org/
[40] Kurganov, A., Tadmor, E., New High-Resolution Central Schemes for Nonlinear Conservation Laws and Convection-Diffusion Equations, *Journal of Computational Physics*, *160* (2000), 1, pp. 241-282
[41] Greenshields, C. J., *et al.*, Implementation of Semi-Discrete, Non-Staggered Central Schemes in a Colocated, Polyhedral, Finite Volume Framework, for High-Speed Viscous Flows, *International Journal for Numerical Methods in Fluids*, *63* (2010), 1, pp. 1-21
[42] Zhang, H., *et al.*, Large Eddy Simulation of Turbulent Supersonic Hydrogen Flames with OpenFOAM, *Fuel*, *282* (2020), 118812
[43] van Leer, B., Towards the Ultimate Conservative Difference Scheme. II. Monotonicity and Conservation Combined in a Second-Order Scheme, *Journal of Computational Physics*, *14* (1974), 4, pp. 361-370
[44] Menter, F., Esch, T., Elements of Industrial Heat Transfer Predictions, *Proceedings*, 16th Brazilian Congress of Mechanical Engineering (COBEM), Uberlandia, Brazil, 2001
[45] Menter, F. R., *et al.*, Ten Years of Industrial Experience with the SST Turbulence Model, *Turbulence, Heat Mass Transfer*, *4* (2003), 1, pp. 625-632
[46] ***, OpenFOAM Foundation, https://cpp.openfoam.org/v9/kOmegaSSTBase_8C_source.html
[47] Chomiak, J., Karlsson, A., Flame Liftoff in Diesel Sprays, *Symposium (International) on Combustion*, *26* (1996), 2, pp. 2557-2564
[48] Vulis, L. A., *Thermal Regimes of Combustion*, McGraw-Hill, New York, USA, 1961
[49] Golovitchev, V. I., *et al.*, 3-D Diesel Spray Simulations Using a New Detailed Chemistry Turbulent Combustion Model, SAE Transactions, 2000-01-1891, 2000
[50] Liu, X., *et al.*, Investigation of Transient Ignition Process in a Cavity Based Scramjet Combustor Using Combined Ethylene Injectors, *Acta Astronautica*, *137* (2017), Aug., pp. 1-7
[51] Cai, Z., *et al.*, Large Eddy Simulation of the Flame Propagation Process in an Ethylene Fueled Scramjet Combustor in a Supersonic Flow, *Proceedings*, 21st AIAA International Space Planes and Hypersonics Technologies Conference, Xiamen, China, 2017
[52] Sun, W., *et al.*, A Path Flux Analysis Method for the Reduction of Detailed Chemical Kinetic Mechanisms, *Combustion and Flame*, *157* (2010), 7, pp. 1298-1307
[53] Pope, S. B., Computationally Efficient Implementation of Combustion Chemistry Using in Situ Adaptive Tabulation, *Combustion Theory and Modelling*, *1* (1997), 1, pp. 41-63
[54] Zheng, S., *et al.*, Effects of Radiation Reabsorption on the Laminar Burning Velocity of Methane/Air and Methane/Hydrogen/Air Flames at Elevated Pressures, *Fuel*, *311* (2022), 122586
[55] Zheng, S., *et al.*, On the Roles of Humidification and Radiation during the Ignition of Ammonia-Hydrogen-Air Mixtures, *Combustion and Flame*, *254* (2023), 112832
[56] Seleznev, R. K., Numerical Investigation of the Ramjet and Scramjet Operation Regimes of the HIFiRE-2 Combustion Chamber, *Fluid Dynamics*, *57* (2022), 6, pp. 758-767
[57] Yang, M., *et al.*, An Experimental and Modeling Study of Ethylene-Air Combustion over a Wide Temperature Range, *Combustion and Flame*, *221* (2020), Nov., pp. 20-40
[58] Huang, Z.-W., *et al.*, Large Eddy Simulation of Flame Structure and Combustion Mode in a Hydrogen Fueled Supersonic Combustor, *International Journal of Hydrogen Energy*, *40* (2015), 31, pp. 9815-9824
[59] Micka, D. J., Driscoll, J. F., Stratified Jet Flames in a Heated (1390K) Air Cross-Flow with Autoignition, *Combustion and Flame*, *159* (2012), 3, pp. 1205-1214
[60] Hu, E., *et al.*, Laminar Flame Speeds and Ignition Delay Times of Methane-Air Mixtures at Elevated Temperatures and Pressures, *Fuel*, *158* (2015), Oct., pp. 1-10
[61] Zettervall, N., *et al.*, Small Skeletal Kinetic Reaction Mechanism for Ethylene-Air Combustion, *Energy & Fuels*, *31* (2017), 12, pp. 14138-14149
[62] Rozenchan, G., *et al.*, Outward Propagation, Burning Velocities, and Chemical Effects of Methane Flames up to 60 ATM, *Proceedings of the Combustion Institute*, *29* (2002), 2, pp. 1461-1470
[63] Lowry, W., *et al.*, Laminar Flame Speed Measurements and Modeling of Pure Alkanes and Alkane Blends at Elevated Pressures, *Journal of Engineering for Gas Turbines and Power*, *133* (2011), 9, 091501
[64] Park, O., *et al.*, Combustion Characteristics of Alternative Gaseous Fuels, *Proceedings of the Combustion Institute*, *33* (2011), 1, pp. 887-894
[65] Park, O., *et al.*, Flame Studies of C_2 Hydrocarbons, *Proceedings of the Combustion Institute*, *34* (2013), 1, pp. 711-718
[66] Jomaas, G., *et al.*, Experimental Determination of Counterflow Ignition Temperatures and Laminar Flame Speeds of C_2-C_3 Hydrocarbons at Atmospheric and Elevated Pressures, *Proceedings of the Combustion Institute*, *30* (2005), 1, pp. 193-200

[67] Hirasawa, T., *et al.*, Determination of Laminar Flame Speeds Using Digital Particle Image Velocimetry: Binary Fuel Blends of Ethylene, *n*-BUTANE, and Toluene, *Proceedings of the Combustion Institute*, *29* (2002), 2, pp. 1427-1434
[68] Egolfopoulos, F. N., *et al.*, Experimental and Numerical Determination of Laminar Flame Speeds: Mixtures of C2-Hydrocarbons with Oxygen and Nitrogen, *Symposium (International) on Combustion*, *23* (1991), 1, pp. 471-478
[69] Hassan, M. I., *et al.*, Properties of Laminar Premixed Hydrocarbon/Air Flames at Various Pressures, *Journal of Propulsion and Power*, *14* (1998), 4, pp. 479-488
[70] Kumar, K., *et al.*, An Experimental Investigation of Ethylene/O_2/Diluent Mixtures: Laminar Flame Speeds with Preheat and Ignition Delays at High Pressures, *Combustion and Flame*, *153* (2008), 3, pp. 343-354
[71] Cong, T. L., Dagaut, P., Experimental and Detailed Kinetic Modeling of the Oxidation of Methane and Methane/Syngas Mixtures and Effect of Carbon Dioxide Addition, *Combustion Science and Technology*, *180* (2008), 10-11, pp. 2046-2091
[72] Jallais, S., *et al.*, An Experimental and Kinetic Study of Ethene Oxidation at a High Equivalence Ratio, *Industrial & Engineering Chemistry Research*, *41* (2002), 23, pp. 5659-5667
[73] Aliyu, M., *et al.*, Effects of Adiabatic Flame Temperature on Flames' Characteristics in a Gas-Turbine Combustor, *Energy*, *243* (2022), 123077
[74] Abdelhafez, A., *et al.*, Adiabatic Flame Temperature for Controlling the Macrostructures and Stabilization Modes of Premixed Methane Flames in a Model Gas-Turbine Combustor, *Energy & Fuels*, *32* (2018), 7, pp. 7868-7877
[75] Wu, Y., *et al.*, A Linearized Error Propagation Method for Skeletal Mechanism Reduction, *Combustion and Flame*, *211* (2020), Jan., pp. 303-311
[76] Zhong, Z., *et al.*, Combustion Characteristics in a Supersonic Combustor with Ethylene Injection Upstream of Dual Parallel Cavities, *Proceedings of the Institution of Mechanical Engineers, Part G: Journal of Aerospace Engineering*, *230* (2016), 13, pp. 2515-2522

Paper submitted: December 23, 2023
Paper revised: March 20, 2024
Paper accepted: March 23, 2024